

Non-resonant Diagrams for Single Production of Top and Bottom Partners

Avik Roy*

National Center for Supercomputing Applications, University of Illinois at Urbana-Champaign

Timothy Andeen[†]

Center for Particles and Fields, Department of Physics, The University of Texas at Austin

February 11, 2022

Abstract

The search for Top and Bottom Partners is a major focus of analyses at both the ATLAS and CMS experiments. When singly produced, these vector-like partners of the Standard Model third generation quarks retain a sizeable cross-section that makes them attractive search candidates in their respective topologies. While most efforts have concentrated on the resonant mode for single production of these hypothetical particles, the most dominant mode at narrow widths, recent studies have revealed a wide and rich phenomenology involving the non-resonant diagrams. In this letter we categorically investigate the impact of the non-resonant diagrams on different Top and Bottom partner single production topologies and their impact on the inclusive cross-section estimation. We also propose a parameterization for calculating the the correction factor to the single vector-like quark production cross-section when such diagrams are included.

1 Introduction

Vector-like Quarks (VLQs) are predicted by a wide variety of Beyond Standard Model (BSM) theories [1, 2, 3, 4, 5, 6, 7, 8, 9, 10] at the TeV scale. With the possible extension of the Standard Model (SM) with a fourth, chiral generation of quarks heavily constrained by precision Higgs measurements [11, 12], VLQs remain a plausible choice for new quarks to extend the SM with additional quarks. Often inspired by the potential solution to the Higgs mass naturalness problem¹, the cut-off scale for new physics is anticipated at the TeV scale when the fine tuning scale for the bare Higgs mass is constrained to $\mathcal{O}(1 - 10)$ [14, 15]. Hence, these hypothetical heavy quarks are prominent search candidates in the post-Higgs discovery era at CERN's Large Hadron Collider (LHC).

In most representations, VLQs are $SU(3)$ color-triplets with strong interactions identical to the SM quarks while their left- and right-chiral representations remain same within the electroweak

*avroy@illinois.edu

[†]tandeen@utexas.edu

¹For a brief review of the naturalness problem for the Higgs boson mass, see Ref. [13].

(EW) symmetry group. The usual four VLQ species are denoted as $X_{+\frac{5}{3}}, T_{+\frac{2}{3}}, B_{-\frac{1}{3}}$ and $Y_{-\frac{4}{3}}$ where the subscript indicates the electric charge of the corresponding particle. Their EW representation identify (T) or (B) singlets, (X, T) , (T, B) , or (B, Y) doublets and (X, T, B) or (T, B, Y) triplets. In most representations, they couple to the Standard Model quarks via exchange of charged (W^+, W^-) or neutral (Z, H) bosons. The interaction of the VLQs with the SM quarks can be summarized with the following simplified Lagrangian [16],

$$\mathcal{L} = \sum_{\zeta, q, Q} \left[\frac{g_w}{2} \sum_V c_{\zeta, V}^{Qq} \bar{Q}_\zeta \not{V} q_\zeta + c_{\zeta, H}^{Qq} H \bar{Q}_\zeta q_\zeta \right] + \text{h.c.} \quad (1)$$

where Q represents the usual VLQs, ζ and ζ' represent alternate chiralities and q represents a SM quark of up or down type. Some of these couplings may be constrained by the conservation of certain quantum numbers. For example, the $+\frac{5}{3}$ charged partner X can only couple with SM up-type quarks by the exchange of a W boson. The usual mass hierarchy of VLQs suggests they interact predominantly with the third generation of the SM quarks [17, 18, 19]. Hence, VLQs are often dubbed Top or Bottom Partners and their interaction with lighter generations set to zero in the simplified representation of Eqn. 1. In this paper, we will generally focus on Top and Bottom partners, denoted by T and B respectively, and unless otherwise stated, the term VLQ will be used interchangeably with T and B .

ATLAS and CMS have performed extensive searches for both pair-produced and singly produced Top and Bottom partners. During Run I of the LHC, at a center of mass energy of 8 TeV, searches for pair production of VLQs were more popular compared to searches for singly produced VLQs [20, 21, 22, 23, 24, 25]. At the lower center of mass energy with the focus of analysis typically confined to VLQ masses less than 1 TeV, the production cross-section of pairs of VLQ is dominant [26]. Additionally, the strong force mediated pair production (Figure 1a) of VLQs becomes a model-independent process and hence the process cross-section only depends on the VLQ mass and not on the species nor its representation. No significant excess was seen in data and exclusion limits on VLQ mass were reported in the range of approximately 600–1000 GeV. These results have served as the benchmark for the Run II searches at 13 TeV center of mass energy. The search effort for single T or B also reported very similar limits in Run I [22, 27].

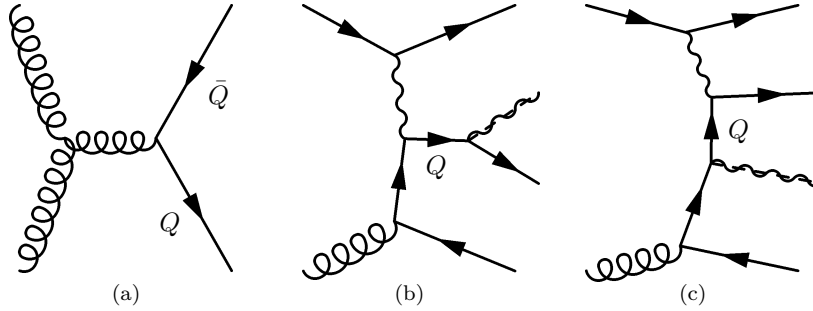


Figure 1: Dominant contributing diagrams for (a) pair production of VLQs, (b) single production of VLQs in s -channel topology, and (c) single production of VLQs in t -channel topology

The Run II ATLAS searches using 36.1fb^{-1} of data from 2015-16 for the pair production of Top and Bottom Partners [28, 29, 30, 31, 32] and their statistical combination [33] set the strongest

current limits on the VLQ masses, excluding $T(B)$ masses up to 1.31 (1.03) TeV for any combination of VLQ branching ratios. Complementary pair production analyses from CMS [34, 35, 36] have also set limits in the range of $\mathcal{O}(1 \text{ TeV})$ for Top and Bottom Partners.

With the region of sensitivity pushed to higher masses, there has been a significant increase in the number of searches for singly produced VLQs [37, 38, 39, 40, 41, 42, 43] during Run II. This is partly because, depending on how strongly VLQs couple with SM bosons and quarks, single production processes can have a larger cross-section at the range of masses that Run II searches have been focusing on [26]. However, unlike pair production, the production of single VLQs is dominated by electroweak processes (Figures 1b,1c). Both kinematics and cross-section of single VLQ processes depend on the representation and the choice of couplings that determine the relative strength of these particles interacting with SM quarks and vector/Higgs bosons. Beyond the usual scope of VLQs at narrow width at small couplings, recent studies have explored VLQ phenomenology at finite width and at next-to-leading-order (NLO) [44, 45, 46, 47, 48]. These studies suggest that extrapolating single VLQ search results performed under the narrow width approximation to large width by parametric recasting alone is neither trivial nor sufficient. A consistent approach for modeling finite width effects requires taking into account the effects of finite width in parton-level simulations.

This paper aims at addressing the relative contribution of resonant (the s -channel in Figure 1b) and nonresonant (the t -channel in Figure 1c) topologies in single VLQ processes at the LHC. In the following section, we investigate the dominant s - and t -channel topologies for different $VQAq$ process where $VQAq$ is short-hand notation for the single production of the VLQ Q being mediated by the vector boson V where the final state includes the boson A and SM quark q . We use a four flavor scheme for parton distributions in the colliding protons. This, along with the assumption of narrow width for all SM bosons and fermions, allows us to factorize the SM particle decays such that they do not impact the parton level kinematic distributions.

2 t -channel topology beyond narrow width

At narrow width, when the couplings are small enough to allow $\frac{\Gamma_Q}{M_Q} \rightarrow 0$, the t -channel diagram has a negligible contribution. However, this contribution can become significant for finite VLQ decay widths. This can be understood by examining the gluon splitting in s - and t -channel diagrams. To illustrate this point, we show the corresponding Feynman diagrams for $WTZt$ and $ZTZt$ processes in Figure 2. As for the $WTZt$ process, the matrix element for the s -channel diagram receives a large contribution from the gluon splitting to a pair of b quarks while the corresponding t -channel diagram is further suppressed by the kinematically less favorable splitting of gluon to a pair of t quarks. In accordance with the findings in Ref. [46], the t -channel consistently remains marginal for all three of the W -mediated produced single- T processes, namely $WTWb$, $WTZt$, and $WTht$.

However, as we look at the $ZTZt$ process diagrams, we note with interest that both s - and t -channel diagrams actually receive a contribution from the same gluon splitting function, i.e. gluon splitting to a pair of top quarks. As we consider larger decay widths for the Top Partner, the relative contribution of the t -channel diagram can make an observable difference, especially when the interference between the two channels is considered.

In order to investigate the impact of t -channel diagrams on single- T and single- B processes, we simulate these processes in MADGRAPH_AMC@NLO [49, 50] using the VLQ UFO model inspired by the parameterization presented in [51]. For each of the $VQAq$ processes with $Q \in \{T, B\}$,

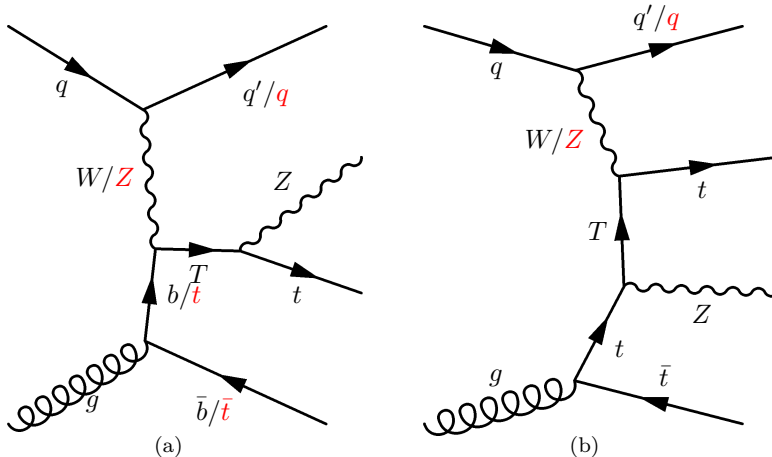


Figure 2: (a) s -channel and (b) t -channel diagrams for $WTZt$ and $ZTZt$ processes.

we generated 20,000 events for M_Q in the range of 1000–2200 GeV in steps of 200 GeV while the relative decay widths are varied between 0.01 and 0.5. The $\kappa, \tilde{\kappa}, \tilde{\kappa}$ parameters introduced in [51] have been calculated from the rescaled couplings $\tilde{c}_W, \tilde{c}_Z, \tilde{c}_H$ introduced in Ref. [48] from a one-to-one correspondence with the tree-level couplings in equation (1) while requiring $\tilde{c}_W = \tilde{c}_Z = \tilde{c}_H$, which would imply almost equal branching ratios in the three decay channels for T and B quarks at the narrow width limit.

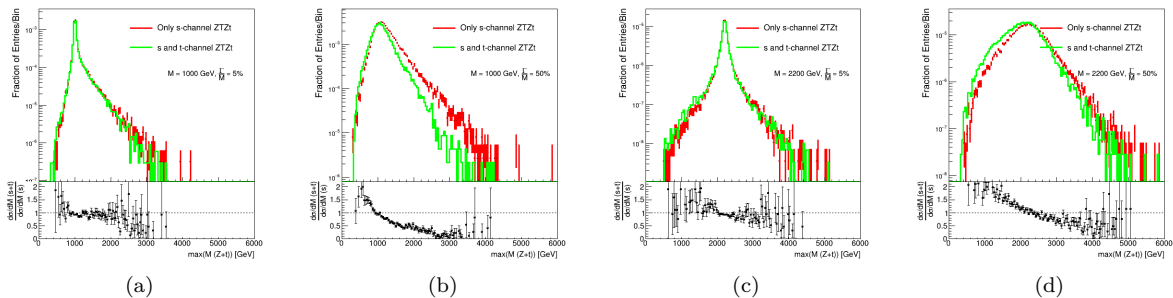


Figure 3: Distribution of the leading invariant mass of the Z boson and the t quark for (a) $M_T = 1.0$ TeV and $\frac{\Gamma}{M} = 0.05$, (b) $M_T = 1.0$ TeV and $\frac{\Gamma}{M} = 0.5$, (c) $M_T = 2.2$ TeV and $\frac{\Gamma}{M} = 0.05$, and (d) $M_T = 2.2$ TeV and $\frac{\Gamma}{M} = 0.5$.

Figure 3 shows the distribution of the leading invariant mass of the Z boson and the t quark in the final state of the $ZTZt$ processes for $M_T = 1.0$ and 2.2 TeV at relative widths of 5% (narrow width) and 50% (large width). As expected, the non-resonant contribution at narrow width (Figures 3a and 3c) is rather minimal and shows up only at the tails of the distributions where the differential cross-section is already suppressed by a few orders of magnitude. However, as larger widths are probed (Figures 3b and 3d), the effect of interference between the s - and t -channel

diagrams become more prominent, causing a clear shift in the differential spectrum.

s - and t -channel gluon splittings	$VQAq$ modes
$b\bar{b}, b\bar{b}$	$WTWb, ZBZb, ZBHb$
$b\bar{b}, t\bar{t}$	$WTHt, WTZt, ZBWt$
$t\bar{t}, b\bar{b}$	$WBHb, ZTWb, WBZb$
$t\bar{t}, t\bar{t}$	$ZTHt, ZTZt, WBWt$

Table 1: Gluon splitting modes in s - and t -channel diagrams for different $VQAq$ processes for single- T and single- B

As the shapes of kinematic distributions associated with T or B quark decay can be significantly affected by the choice of contribution from non-resonant diagrams with similar gluon splitting diagrams, it is even more interesting to investigate similar impacts when the t -channel diagram receives a contribution from gluon splitting to $b\bar{b}$ while the resonant contribution of the s -channel diagram receives contribution from the t -channel diagram. The gluon splitting modes of different $VQAq$ processes are listed in Table 1. Both $ZTWb$ and $WBZb$ modes require the presence of a gluon splitting to $b\bar{b}$ in the non-resonant diagram and a $t\bar{t}$ splitting for the resonant diagram in s -channel. The differential cross-section with respect to the leading invariant masses of $W + b$ and $Z + b$ for these processes are shown in Figure 4. The usual assumption of a negligible impact of t -channel still holds for these processes (Figures 4a , 4c , 4e and 4g). In this case the t -channel contribution is only apparent in the low mass tail. Here the differential cross-section is up to two orders of magnitude smaller than what is found near the peak of the distribution. However, at larger widths (Figures 4b , 4d , 4f and 4h), these distributions receive a sizeable non-resonant contribution at the lower mass tails. It is apparent that these contributions not only change the shape of the overall distribution but also introduces a sizeable increase in the process cross-section overall.

It is now clear that the t -channel can make a sizeable contribution to the cross-section when the gluon splitting function has a large contribution for the non-resonant diagrams at large width. This effect will become further amplified when considering the H -associated final states for single VLQ processes. As described in Ref. [46], the resonant cross-section for single VLQ processes with Higgs associated final states includes an extra factor of $\frac{1}{s}$ that amplifies the differential cross-section at lower energies. This extra boost can be further amplified when coupled with t -channel diagrams that come with a comparable (or dominant) gluon splitting function. From Table 1, we can see that both s - and t -channel diagrams for $ZBHb$ ($ZTHt$) have a gluon splitting to $b\bar{b}$ ($t\bar{t}$), while the t -channel gluon splitting to $b\bar{b}$ for $WBHb$ has a dominant contribution compared to s -channel's $t\bar{t}$. In Figure 5, we show the distributions for invariant mass of the leading $H + b$ for $WBHb$ and $ZBHb$ processes as well as the distribution for leading $H + t$ invariant mass distribution for $ZTHt$. In these cases, the low mass tail can have a significant contribution even at not-so-narrow widths, and the overall production cross-section can become significantly larger than what is seen from s -channel production alone.

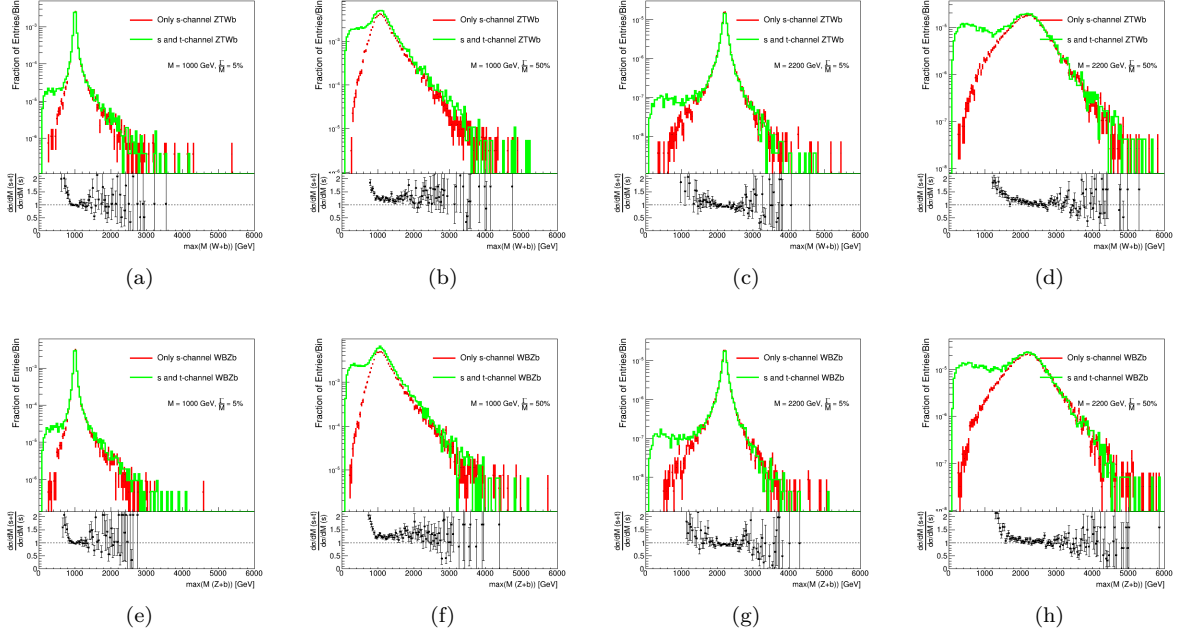


Figure 4: Distribution of the leading $W + b$ (top row, for $ZTWb$) and $Z + b$ (bottom row, for $WBZb$) invariant masses for (a), (e) $M_{T/B} = 1.0$ TeV and $\frac{\Gamma}{M} = 0.05$, (b), (f) $M_{T/B} = 1.0$ TeV and $\frac{\Gamma}{M} = 0.5$, (c), (g) $M_{T/B} = 2.2$ TeV and $\frac{\Gamma}{M} = 0.05$, (d), (h) $M_{T/B} = 2.2$ TeV and $\frac{\Gamma}{M} = 0.5$.

3 Parameterized cross-section estimate for single VLQ processes

At narrow width, single VLQ process cross-sections can be estimated with a factorization of couplings and branching ratios [16, 48]-

$$\sigma_{VQAq,NWA} = \tilde{c}_V^2 \times \sigma_{VQ}(\tilde{c}_V = 1) \times \text{BR}(Q \rightarrow Aq). \quad (2)$$

At larger decay widths for T and B quarks, the cross-section estimate of Eqn. 2 needs to be modified. In Ref. [48], a parameterized correction for the s -channel cross-section estimate has been formulated that modifies the factorized cross-section calculation as

$$\sigma_{VQAq,s} = \frac{1}{P_{NWA}(M_Q, \vec{c})} \times \tilde{c}_V^2 \times \sigma_{VQ}(\tilde{c}_V = 1) \times \text{BR}(Q \rightarrow Aq). \quad (3)$$

When the t -channel contribution becomes significant, the estimate from Eqn. 3 needs to be further revised. Therefore we introduce a parameterized cross-section correction $F_{t,VQAq}(M_Q, \frac{\Gamma_Q}{M_Q})$, defined as-

$$F_{t,VQAq}\left(M_Q, \frac{\Gamma_Q}{M_Q}\right) = \frac{\sigma_{VQAq,s+t}}{\sigma_{VQAq,s}}. \quad (4)$$

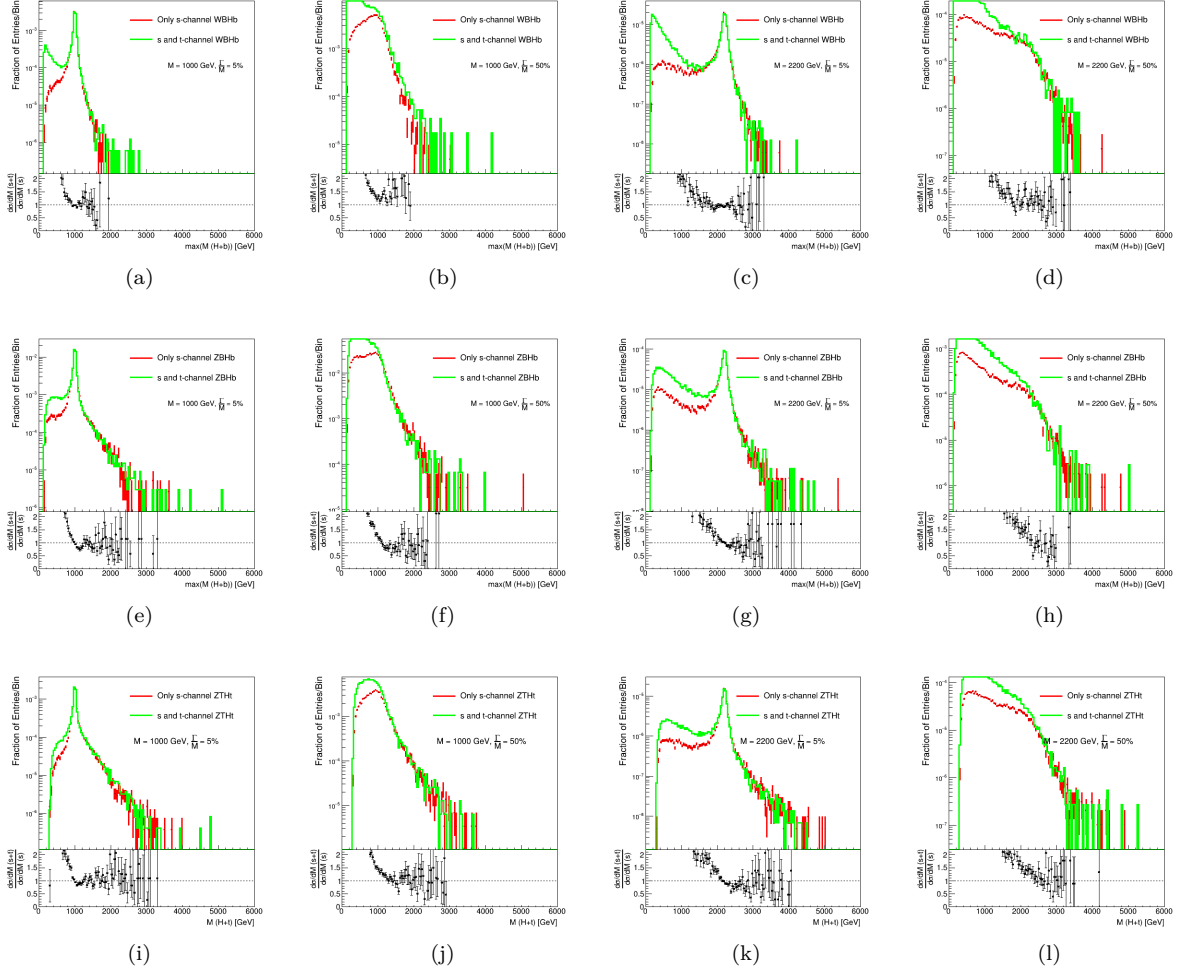


Figure 5: Distribution of the leading $H + b$ (top row, for $WBHb$ and middle row, for $ZBHb$) and $H + t$ (bottom row, for $ZTHt$) invariant masses for (a), (e), (i), $M_{T/B} = 1.0$ TeV and $\frac{\Gamma}{M} = 0.05$, (b), (f), (j), $M_{T/B} = 1.0$ TeV and $\frac{\Gamma}{M} = 0.50$, (c), (g), (k), $M_{T/B} = 2.2$ TeV and $\frac{\Gamma}{M} = 0.05$, and (d), (h), (l), $M_{T/B} = 1.0$ TeV and $\frac{\Gamma}{M} = 0.50$,

Following the arguments presented in the previous section and also in Ref. [46], we consider the effect of t -channel contribution of $WTWb$, $WTZt$, $WTHt$, and $ZBWt$ processes to be marginal and use $F_{t,VQAq} \approx 1$ for these processes. For the processes where the t -channel contribution is large, we use the cross-section estimate from the MADGRAPHAMC@NLO simulations described in Section 2. Figure 6 shows the distribution of the $F_{t,VQAq}$ factor as a function of VLQ mass and relative decay widths. It can be seen that there appears to be a lack of continuity, or cutoff, at $\frac{\Gamma}{M} = 0.1$ in these simulations. This cutoff is an artifact of the choice of dynamic scale for the cross-section calculations, determined by MADGRAPHAMC@NLO. The default dynamic scale for these

simulations was chosen based on the CKKW scheme [52, 53]. The MADGRAPH implementation of this scale choice can vary when particle records with $\frac{\Gamma}{M} > 10\%$ are present in the process which can appear as an scale-dependent uncertainty in the estimation of cross-sections ². This unphysical, computational effect introduces an uncertainty of $\mathcal{O}(10\%)$ at the relative decay width threshold of 10%.

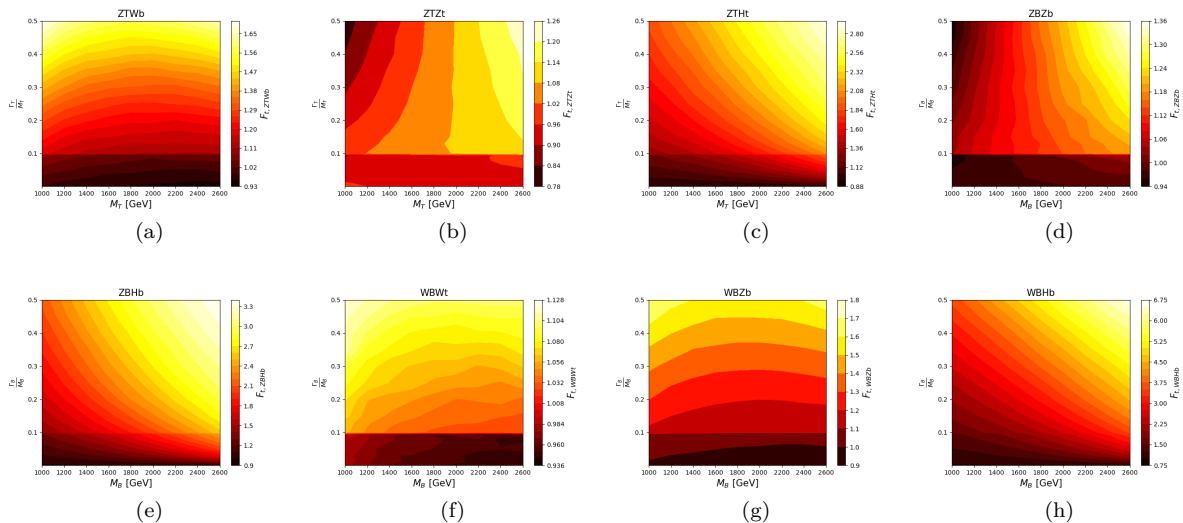


Figure 6: Calculated values of $F_{VQAq,t}(M_Q, \frac{\Gamma_Q}{M_Q})$ for (a) $ZTWb$, (b) $ZTZt$, (c) $ZTHt$, (d) $ZBZb$, (e) $ZBHb$, (f) $WBWt$, (g) $WBZb$, and (h) $WBHb$ processes.

To obtain parameterized representation of $F_{t,VQAq}$, we independently perform a linear least squared error fit for $\frac{\Gamma}{M} < 0.1$ and a second order polynomial fit for $\frac{\Gamma}{M} \geq 0.1$ for each VLQ mass point simulated (Eqn. 5).

$$F_{t,VQAq} \left(M_Q, \frac{\Gamma_Q}{M_Q} \right) = \begin{cases} A_l + B_l \frac{\Gamma_Q}{M_Q}, & \frac{\Gamma_Q}{M_Q} < 0.1 \\ A_h + B_h \frac{\Gamma_Q}{M_Q} + C_h \left(\frac{\Gamma_Q}{M_Q} \right)^2, & \frac{\Gamma_Q}{M_Q} \geq 0.1 \end{cases} \quad (5)$$

The difference between the fitted polynomials at $\frac{\Gamma}{M} = 0.1$ is treated as an uncertainty associated with the scale dependence of the cross-section estimate for $VQAq$ processes. The best fit values for the parameters in Eqn. 5 are given in Table 2 and Table 3 for $\frac{\Gamma}{M} < 0.1$ and $\frac{\Gamma}{M} \geq 0.1$ respectively.

4 Conclusion

This letter has thoroughly investigated the effects of non-resonant diagrams on physical distributions of single Top and Bottom partner production at parton level as well as cross-section estimation. Our investigation suggests that the relative strength of the gluon splitting function in the s - and

²This observation has been discussed with MADGRAPH authors and can be followed at <https://bugs.launchpad.net/mg5amcnlo/+bug/1943581>.

	$M_{T/B}$ [TeV]	$ZTWb$	$ZTZt$	$ZTHt$	$ZBZb$	$ZBHb$	$WBWt$	$WBZb$	$WBHb$
A_t	1.0	0.984	0.969	0.975	0.973	0.981	0.977	0.982	0.981
	1.2	0.972	0.959	0.965	0.975	0.987	0.969	0.970	0.978
	1.4	0.966	0.954	0.962	0.974	0.991	0.960	0.966	0.979
	1.6	0.959	0.951	0.963	0.977	1.002	0.956	0.963	0.985
	1.8	0.958	0.948	0.966	0.976	1.021	0.954	0.957	0.997
	2.0	0.951	0.945	0.972	0.979	1.043	0.950	0.952	1.017
	2.2	0.950	0.944	0.984	0.980	1.077	0.949	0.949	1.058
	2.4	0.944	0.937	1.002	0.978	1.118	0.946	0.942	1.108
	2.6	0.947	0.938	1.032	0.977	1.176	0.944	0.944	1.195
B_t	1.0	1.091	-0.748	2.204	-0.275	3.237	0.136	1.045	4.920
	1.2	0.959	-0.471	2.807	-0.103	4.196	0.084	0.983	6.206
	1.4	0.860	-0.373	3.391	-0.029	5.335	0.113	0.853	7.746
	1.6	0.849	-0.219	4.117	0.046	6.517	0.105	0.767	9.714
	1.8	0.799	-0.108	4.958	0.178	7.809	0.076	0.805	12.063
	2.0	0.819	0.029	5.932	0.240	9.281	0.118	0.843	14.751
	2.2	0.849	0.071	7.057	0.348	10.727	0.110	0.810	17.689
	2.4	0.925	0.332	8.243	0.490	12.249	0.098	0.896	21.054
	2.6	0.909	0.409	9.514	0.582	13.678	0.155	0.963	24.442

Table 2: Best fit values of the parameters in estimating F_t from Eqn. 5 for $\frac{\Gamma}{M} < 0.1$

t -channel diagrams plays a decisive role in determining the qualitative nature of the impact of non-resonant diagrams in these processes. We additionally evaluate a parameterized correction factor for the inclusive cross-section estimation of these processes. Such factorizable parameterization can facilitate model-independent interpretation of single VLQ searches allowing a harmonized and consistent platform for combination of such searches at the LHC.

	$M_{T/B}$ [TeV]	$ZTWb$	$ZTZt$	$ZTHt$	$ZBZb$	$ZBHb$	$WBWt$	$WBZb$	$WBHb$
A_h	1.0	1.070	1.068	1.122	1.067	1.147	1.035	1.070	1.126
	1.2	1.055	1.078	1.145	1.082	1.206	1.030	1.050	1.162
	1.4	1.040	1.076	1.165	1.095	1.282	1.025	1.053	1.234
	1.6	1.035	1.080	1.222	1.103	1.376	1.025	1.042	1.335
	1.8	1.028	1.090	1.274	1.109	1.491	1.017	1.025	1.457
	2.0	1.039	1.083	1.373	1.113	1.638	1.018	1.041	1.699
	2.2	1.029	1.098	1.471	1.130	1.828	1.015	1.030	1.923
	2.4	1.027	1.102	1.595	1.139	2.006	1.010	1.019	2.289
2.6	1.020	1.101	1.771	1.130	2.217	1.006	1.029	2.689	
B_h	1.0	1.049	-0.708	2.132	-0.274	2.764	0.219	1.028	4.223
	1.2	0.898	-0.588	2.447	-0.175	3.334	0.144	0.919	5.133
	1.4	0.835	-0.384	2.926	-0.089	3.812	0.130	0.743	6.038
	1.6	0.802	-0.238	3.199	0.010	4.312	0.107	0.729	7.111
	1.8	0.771	-0.175	3.638	0.125	4.626	0.126	0.775	8.236
	2.0	0.653	0.015	3.783	0.286	4.756	0.103	0.627	8.735
	2.2	0.706	0.027	4.029	0.280	4.559	0.106	0.710	9.749
	2.4	0.735	0.134	4.117	0.357	4.461	0.128	0.821	9.685
2.6	0.814	0.275	3.777	0.613	4.092	0.190	0.748	9.564	
C_h	1.0	0.428	0.367	-1.318	0.056	-1.623	-0.087	0.487	1.354
	1.2	0.534	0.358	-1.469	0.042	-2.180	0.041	0.512	0.905
	1.4	0.575	0.185	-2.013	0.036	-2.656	0.059	0.704	0.417
	1.6	0.575	0.105	-2.207	0.019	-3.315	0.085	0.676	-0.576
	1.8	0.616	0.150	-2.760	-0.034	-3.752	0.067	0.628	-1.710
	2.0	0.855	-0.031	-2.931	-0.181	-4.005	0.114	0.898	-2.081
	2.2	0.838	0.116	-3.327	-0.035	-3.824	0.123	0.816	-3.627
	2.4	0.884	0.078	-3.554	-0.005	-3.876	0.105	0.706	-3.455
2.6	0.884	-0.012	-3.074	-0.318	-3.565	-0.002	0.981	-3.511	

Table 3: Best fit values of the parameters in estimating F_t from Eqn. 5 for $\frac{\Gamma}{M} \geq 0.1$

Acknowledgment

This work is supported by the U.S. Department of Energy, Office of High Energy Physics under Grant No. DE-SC0007890.

References

- [1] F Del Aguila and Mark J Bowick. The possibility of new fermions with $\Delta I=0$ mass. Nucl. Phys. B, 224(1):107–136, 1983.
- [2] David B Kaplan, Howard Georgi, and Savvas Dimopoulos. Composite Higgs scalars. Phys. Lett. B, 136(3):187–190, 1984.
- [3] Kaustubh Agashe, Roberto Contino, and Alex Pomarol. The minimal composite Higgs model. Nucl. Phys. B, 719(1-2):165–187, 2005.
- [4] Roberto Contino, Leandro Da Rold, and Alex Pomarol. Light custodians in natural composite Higgs models. Phys. Rev. D, 75(5):055014, 2007.
- [5] Nima Arkani-Hamed, Andrew G Cohen, Emanuel Katz, and Ann E Nelson. The littlest Higgs. J. High Energy Phys., 2002(07):034, 2002.
- [6] Yutaka Hosotani, Shusaku Noda, and Kazunori Takenaga. Dynamical gauge-Higgs unification in the electroweak theory. Phys. Lett. B, 607(3-4):276–285, 2005.
- [7] Ignatios Antoniadis, Karim Benakli, and Mariano Quirós. Finite Higgs mass without supersymmetry. New Journal of Physics, 3(1):20, 2001.
- [8] Thomas Appelquist, Hsin-Chia Cheng, and Bogdan A Dobrescu. Bounds on universal extra dimensions. Phys. Rev. D, 64(3):035002, 2001.
- [9] F Del Aguila, Ll Ametller, Gordon L Kane, and Jorge Vidal. Vector-like fermion and standard Higgs production at hadron colliders. Nucl. Phys. B, 334(1):1–23, 1990.
- [10] Juan Antonio Aguilar-Saavedra. Identifying Top partners at LHC. J. of High Energy Phys., 2009(11):030, 2009.
- [11] Otto Eberhardt, Geoffrey Herbert, Heiko Lacker, Alexander Lenz, Andreas Menzel, Ulrich Nierste, and Martin Wiebusch. Impact of a Higgs boson at a mass of 126 GeV on the standard model with three and four fermion generations. Physical Review Letters, 109(24):241802, 2012.
- [12] Eric Kuflik, Yosef Nir, and Tomer Volansky. Implications of Higgs searches on the four-generation standard model. Physical review letters, 110(9):091801, 2013.
- [13] James D Wells. Higgs naturalness and the scalar boson proliferation instability problem. Synthese, 194(2):477–490, 2017.
- [14] M Schmaltz. Little Higgs goes to TASI. In Physics In $D \geq 4$ Tasi 2004: TASI 2004, pages 463–492. World Scientific, 2006.

- [15] Laura Reina. TASI 2011: Lectures on Higgs-boson physics. [arXiv preprint arXiv:1208.5504](#), 2012.
- [16] Oleksii Matsedonskyi, Giuliano Panico, and Andrea Wulzer. On the interpretation of Top partners searches. [J. High Energy Phys.](#), 2014(12):97, 2014.
- [17] Yasuhiro Okada and Luca Panizzi. LHC signatures of vector-like quarks. [Advances in High Energy Physics](#), 2013, 2013.
- [18] Juan Antonio Aguilar-Saavedra. Mixing with vector-like quarks: constraints and expectations. In [EPJ Web of Conferences](#), volume 60, page 16012. EDP Sciences, 2013.
- [19] Juan Antonio Aguilar-Saavedra, Daniel E López-Fogliani, and C Muñoz. Novel signatures for vector-like quarks. [J. of High Energy Phys.](#), 2017(6):95, 2017.
- [20] The ATLAS Collaboration. Search for production of vector-like quark pairs and of four top quarks in the lepton-plus-jets final state in pp collisions at $\sqrt{s} = 8$ TeV with the ATLAS detector. [J. High Energy Phys.](#), 2015(8):105, 2015.
- [21] The ATLAS Collaboration. Search for vectorlike B quarks in events with one isolated lepton, missing transverse momentum, and jets at $s = 8$ TeV with the ATLAS detector. [Phys. Rev. D](#), 91(11):112011, 2015.
- [22] The ATLAS Collaboration. Search for pair and single production of new heavy quarks that decay to a Z boson and a third-generation quark in pp collisions at $\sqrt{s} = 8$ TeV with the ATLAS detector. [J. High Energy Phys.](#), 2014(11):a104, 2014.
- [23] The CMS Collaboration. Search for vectorlike charge 2/3 T quarks in proton-proton collisions at $\sqrt{s} = 8$ TeV. [Phys. Rev. D](#), 93(1):012003, 2016.
- [24] The CMS Collaboration. Search for pair-produced vectorlike B quarks in proton-proton collisions at $\sqrt{s} = 8$ TeV. [Phys. Rev. D](#), 93(11):112009, 2016.
- [25] The CMS Collaboration. Search for top-quark partners with charge 5/3 in the same-sign dilepton final state. [Phys. Rev. Lett.](#), 112(17):171801, 2014.
- [26] Juan Antonio Aguilar-Saavedra, Rachid Benbrik, Sven Heinemeyer, and Manuel Pérez-Victoria. Handbook of vectorlike quarks: Mixing and single production. [Phys. Rev. D](#), 88(9):094010, 2013.
- [27] The ATLAS Collaboration. Search for single production of vector-like quarks decaying into Wb in pp collisions at $\sqrt{s} = 8$ TeV with the ATLAS detector. [Eur. Phys. J. C](#), 76(8):442, 2016.
- [28] The ATLAS Collaboration. Search for pair production of up-type vector-like quarks and for four-top-quark events in final states with multiple b-jets with the ATLAS detector. [J. High Energy Phys.](#), 2018(7):89, 2018.
- [29] The ATLAS Collaboration. Search for pair production of heavy vector-like quarks decaying to high-pT W bosons and b quarks in the lepton-plus-jets final state in pp collisions at $\sqrt{s} = 13$ TeV with the ATLAS detector. [J. High Energy Phys.](#), 2017(10):141, 2017.

- [30] The ATLAS Collaboration. Search for pair production of vector-like top quarks in events with one lepton, jets, and missing transverse momentum in $\sqrt{s} = 13$ TeV pp collisions with the ATLAS detector. J. High Energy Phys., 2017(8):52, 2017.
- [31] The ATLAS Collaboration. Search for new phenomena in events with same-charge leptons and b-jets in pp collisions at $\sqrt{s} = 13$ TeV with the ATLAS detector. J. High Energy Phys., 2018(12):39, 2018.
- [32] The ATLAS Collaboration. Search for pair production of heavy vectorlike quarks decaying into hadronic final states in pp collisions at $\sqrt{s} = 13$ TeV with the ATLAS detector. Phys. Rev. D, 98(9):092005, 2018.
- [33] The ATLAS Collaboration. Combination of the searches for pair-produced vectorlike partners of the third-generation quarks at $s = 13$ TeV with the ATLAS detector. Phys. Rev. Lett., 121(21):211801, 2018.
- [34] The CMS Collaboration. Search for pair production of vector-like T and B quarks in single-lepton final states using boosted jet substructure in proton-proton collisions at $\sqrt{s} = 13$ TeV. J. High Energy Phys., 2017(11):085, 2017.
- [35] The CMS Collaboration. Search for pair production of vector-like quarks in the $bW\bar{b}W$ channel from proton-proton collisions at $\sqrt{s} = 13$ TeV. Phys. Lett. B, 779:82–106, 2018.
- [36] The CMS Collaboration. Search for vector-like T and B quark pairs in final states with leptons at $\sqrt{s} = 13$ TeV. J. High Energy Phys., 2018(8):177, 2018.
- [37] The ATLAS Collaboration. Search for pair and single production of vectorlike quarks in final states with at least one Z boson decaying into a pair of electrons or muons in pp collision data collected with the ATLAS detector at $\sqrt{s} = 13$ TeV. Phys. Rev. D, 98(11):112010, 2018.
- [38] The ATLAS Collaboration. Search for single production of vector-like quarks decaying into Wb in pp collisions at $\sqrt{s} = 13$ TeV with the ATLAS detector. J. High Energy Phys., 2019(5):164, 2019.
- [39] The ATLAS Collaboration. Search for large missing transverse momentum in association with one top-quark in proton-proton collisions at $\sqrt{s} = 13$ TeV with the ATLAS detector. J. High Energy Phys., 2019(5):41, 2019.
- [40] The CMS Collaboration. Search for single production of a vector-like T quark decaying to a Z boson and a top quark in proton-proton collisions at $\sqrt{s} = 13$ TeV. Phys. Lett. B, 781:574–600, 2018.
- [41] The CMS Collaboration. Search for single production of vector-like quarks decaying to a top quark and a W boson in proton-proton collisions at $\sqrt{s} = 13$ TeV. The European Physical Journal. C, 79(2):90, 2019.
- [42] The CMS Collaboration. Search for single production of vector-like quarks decaying to a b quark and a Higgs boson. J. High Energy Phys., 2018(6):31, 2018.
- [43] The CMS Collaboration. Search for electroweak production of a vector-like T quark using fully hadronic final states. J. High Energy Phys., 2020(1):36, 2020.

- [44] Stefano Moretti, Dermot O’Brien, Luca Panizzi, and Hugo Prager. Production of extra quarks at the Large Hadron Collider beyond the narrow width approximation. Physical Review D, 96(7):075035, 2017.
- [45] Alexandra Carvalho, Stefano Moretti, Dermot O’Brien, Luca Panizzi, and Hugo Prager. Single production of vectorlike quarks with large width at the Large Hadron Collider. Phys. Rev. D, 98(1):015029, 2018.
- [46] Aldo Deandrea, Thomas Flacke, Benjamin Fuks, Luca Panizzi, and Hua-Sheng Shao. Single production of vector-like quarks: the effects of large width, interference and NLO corrections. arXiv preprint arXiv:2105.08745, 2021.
- [47] Giacomo Cacciapaglia, Alexandra Carvalho, Aldo Deandrea, Thomas Flacke, Benjamin Fuks, Devdatta Majumder, Luca Panizzi, and Hua-Sheng Shao. Next-to-leading-order predictions for single vector-like quark production at the lhc. Physics Letters B, 793:206–211, 2019.
- [48] Avik Roy, Nikiforos Nikiforou, Nuno Castro, and Timothy Andeen. Novel interpretation strategy for searches of singly produced vectorlike quarks at the LHC. Physical Review D, 101(11):115027, 2020.
- [49] Johan Alwall, R Frederix, S Frixione, V Hirschi, Fabio Maltoni, Olivier Mattelaer, H-S Shao, T Stelzer, P Torrielli, and M Zaro. The automated computation of tree-level and next-to-leading order differential cross sections, and their matching to parton shower simulations. J. High Energy Phys., 2014(7):79, 2014.
- [50] Johan Alwall, Michel Herquet, Fabio Maltoni, Olivier Mattelaer, and Tim Stelzer. MadGraph 5: going beyond. J. High Energy Phys., 2011(6):128, 2011.
- [51] Benjamin Fuks and Hua-Sheng Shao. QCD next-to-leading-order predictions matched to parton showers for vector-like quark models. Eur. Phys. J. C, 77(2):135, 2017.
- [52] Stefano Catani, Frank Krauss, Bryan R Webber, and Ralf Kuhn. QCD matrix elements+parton showers. Journal of High Energy Physics, 2001(11):063, 2002.
- [53] Frank Krauss. Matrix elements and parton showers in hadronic interactions. Journal of High Energy Physics, 2002(08):015, 2002.